**Title**
Electrodeposited, Transverse Nanowire Electroluminescent Junctions



**Author**
Qiao, Shaopeng

**Publication Date**
2018

Peer reviewed|Thesis/dissertation

UNIVERSITY OF CALIFORNIA,
IRVINE

# Electrodeposited, Transverse Nanowire Electroluminescent Junctions

THESIS

submitted in partial satisfaction of the requirements
for the degree of

MASTER OF SCIENCE

in Physics

by

Shaopeng Qiao

Thesis Committee:
Professor Reginald M. Penner , Chair
Professor Ilya N. Krivorotov
Assistant Professor Shane Ardo

2018

# DEDICATION

To my parents and friends.

# TABLE OF CONTENTS

# LIST OF FIGURES

Page

# LIST OF TABLES

# ACKNOWLEDGMENTS

I would like to thank my thesis advisor Professor Reginald M. Penner. With his support, I have learned a lot about electrochemisty, different materials characterization techniques and light emitting devices. He is always very helpful when people come to him and gives out greas advices. He showed great supports for my job hungtings and always looks out opportunities for me. Without him, I would not be able to have all the achievements in my graduate school.

I would like to thank my committee member Professor Ilya N. Krivorotov and Professor Shane Ardo for being on my master thesis committee. Thanks for the patience during the communications and the efforts on my thesis.

I would like to thank my funding agency National Science Foundation, Division of Materials Research through contract DMR-1206867. All the SEM and XRD data were acquired using instrumentation of the LEXI facility (lexi.eng.uci.edu/) at UCI and PL spectra were acquired at the Laser Spectroscopy Facility (LSF) at the Department of Chemistry at UCI. I would like to Dr. Dmitry Fishman, Director of the UCI Chemistry Laser Spectroscopy Facility, for his expert assistance. I would like to thank Professor Rob Corn and his students for providing access to the microscope and CMOS camera used for EL measurements.

I would like to thank all the other members in Penner group especially Dr. Qiang Xu, Dr. Rajen K. Dutta, Dr. Mya Le Thai, Dr Xiaowei Li. for valuable discussions on my research. And also thanks to Alex Fast and Kevin T. Crampton for the help on spectrometer setup.

I would like to thank American Chemical Society for giving me the permission to incorporate my previously published work in ACS Nano into my thesis.

# ABSTRACT OF THE THESIS

Electrodeposited, Transverse Nanowire Electroluminescent Junctions

By

Shaopeng Qiao

Master of Science in Physics

University of California, Irvine, 2018

Professor Reginald M. Penner , Chair

The preparation by electrodeposition of transverse nanowire electroluminescent junctions (*tn-ELJs*) is described and the electroluminescence ($EL$) properties of these devices are characterized. The lithographically patterned nanowire electrodeposition process (LPNE) is first used to prepare a long (mm's), linear, nanocrystalline CdSe nanowires on glass. The thickness of these nanowires along the emission axis is 60 nm and the width, $w_{CdSe}$, along the electrical axis is adjustable from 100 - 450 nm. Ten pairs of nickel-gold electrical contacts are then positioned along the axis of this nanowire using lithographically directed electrodeposition. The resulting linear array of nickel-CdSe-gold junctions produce electroluminescence (EL) with an external quantum efficiency, $EQE$, and threshold voltage, $V_{th}$, that depends sensitively on $w_{CdSe}$. $EQE$ increases with increasing electric field and also with increasing $w_{CdSe}$, and $V_{th}$ also increases with $w_{CdSe}$, and therefore the electrical resistance, of the *tn-ELJs*. $V_{th}$ down to 1.8($\pm$0.2)V (for $w_{CdSe}$ $\approx$100 nm) and $\eta_{EL}$ of 5.5($\pm$0.5) $\times$ $10^{-5}$ (for $w_{CdSe}$ $\approx$450 nm) are obtained. *tn-ELJs* produce a broad $EL$ emission envelope, spanning the wavelength range from 600 - 960 nm.

# Chapter 1

# Introduction

## 1.1 Electroluminescence from Electrodeposited Semiconductor Nanostructures



Methods for patterning nanometer-scale electroluminescent ($EL$) structures on surfaces will be required for a variety of anticipated device applications ranging from chemical sensors, to information transfer and processing, and interfaces to biological systems.[61, 31, 62] Single semiconductor nanostructures were first electrically stimulated to emit light in 2001 when Lieber and coworkers reported light emission at the forward-biased junctions between crossed n-doped and p-doped InP nanowire junctions.[16] Many creative device architectures for nanostructure $EL$ devices have subsequently been demonstrated based upon single nanowires,[3, 68, 69, 14, 18] nanowire arrays interfaced to films,[64, 19, 6] crossed nanowire p-n junctions,[21, 23, 67] and core-shell hetrostructures,[44, 57, 20, 29, 5] In the specific

case of devices based upon cadmium selenide (CdSe) - the semiconductor of interest here - external quantum efficiencies ($EQE$s) are generally in the $10^{-7}$ to $10^{-5}$ range (Table 1.1).

Work on *films* of thousands or millions of semiconductor nanocrystals preceded experiments on single nanostructures. These films are macroscopic in two dimensions, and nanoscopic in the third, or thickness dimension. Bulovic and coworkers first demonstrated that layers of CdSe nanocrystals could produce $EL$ in 1992.[10] Although $EQE$ for these devices were initially as low as those seen for emissive devices based upon single semiconductor nanostructures,[12, 11] it was soon discovered that the insertion of hole-transporting layers (e.g. PEDOT) and electron-injecting layers (e.g. ZnO) sandwiching the emitting layer elevated the $EQE$ to 1% or higher,[27, 66, 22, 40, 63] (for recent reviews, see: [48, 54]).

By comparison, there has been little work involving $EL$ from *electrodeposited* semiconductor nanostructures.[41, 60, 1] But electrodeposition provides capabilities for device fabrication that are complimentary to those enabled using chemically synthesized nanocrystals or single crystalline nanowires, including the ability to pattern and position emitter structures with high precision.[41] Here, we describe a discovery platform that provides a means for electrodepositing and characterizing the $EL$ properties of linear arrays of many nearly identical metal-semiconductor-metal (M-S-M) junctions. In this work, we use this platform to characterize arrays of nickel-(*nc*-CdSe)-gold M-S-M junctions. These junctions are prepared by first electrodepositing an ensemble of 60 nearly identical *nc*-CdSe nanowires, and then locating nickel and gold contacts on opposite sides of each nanowire along their axes also using electrodeposition. These devices are termed "transverse nanowire electroluminescent junctions" or *tn-ELJs*.

Table 1.1: Performance of CdSe Nanostructure-Based Electroluminescent Junctions

| Junction Description[a] | Electrode Spacing (nm) | $V_{th}$[b] (V) | Spectral Range (nm) | $EQE_{max}$[c] | Ref |
|---|---|---|---|---|---|
| **nanocrystal films** | | | | | |
| CdSe QD | 1000 | 4 | 480-650 | $1\text{-}10\times10^{-5}$ | [11] |
| CdSe QD-PVK | 70-120 | 5-7 | 615-650 | $5\times10^{-6}$ | [12] |
| CdSe QD-TPD | 40 | 3 | 540-590 | $5.2\times10^{-3}$ | [10] |
| CdSe-CdS core-shell QD | - - | 4 | 600-630 | $4\text{-}8\times10^{-3}$ | [66] |
| CdSe-CdS core-shell QD | - - | 1.5 | 600-635 | 12-18 | [30] |
| CdSe QD TPD | - - | 15.5 | 400-750 | $1.4\times10^{-6}$ | [46] |
| **single nanostructures** | | | | | |
| CdSe NR | 30 | $1.7(\pm0.1)$ | 650-820 | $10^{-5}$ | [18] |
| CdSe NW | 2000-6000 | 4 | 620-850 | $(1\text{-}5)\times10^{-6}$ | [14] |
| ***nc*-CdSe in a nanogap** | | | | | |
| nanocrystals | 100-500 | $1.6-1.8$ | 580-720 | - - | [15] |
| $T_{dep} = 20°C$ | 200 | $1.9(\pm0.1)$ | - - | $1.2(\pm0.4)\times10^{-6}$ | [60] |
| $T_{dep} = 75°C$ | 200 | $1.5(\pm0.2)$ | 650-890 | $1.8(\pm0.7)\times10^{-6}$ | [60] |
| ***nc*-CdSe NW arrays** | | | | | |
| annealed 300°C×4h | 5000 | $16(\pm5)$ | - - | $6(\pm2)\times10^{-7}$ | [1] |
| annealed 450°C×1h | 5000 | $12(\pm1)$ | - - | $8(\pm2)\times10^{-7}$ | [1] |
| annealed 300°C×4h | 600 | $6.2(\pm0.5)$ | 610-890 | $4(\pm1)\times10^{-6}$ | [1] |
| **CdSe *tn-ELJ*** | **102** | **$1.85(\pm0.06)$** | 570-860 | **$1.3(\pm0.1)\times10^{-5}$** | **This work** |
| | **195** | **$3.8(\pm0.4)$** | 660-960+ | **$2.4(\pm0.1)\times10^{-5}$** | ” |
| | **313** | **$5.1(\pm0.3)$** | 600-960+ | **$2.5(\pm0.1)\times10^{-5}$** | ” |
| | **398** | **$6.0(\pm0.5)$** | 550-960+ | **$3.6(\pm0.2)\times10^{-5}$** | ” |
| | **448** | **$6.9(\pm0.3)$** | 560-960+ | **$4.9(\pm0.2)\times10^{-5}$** | ” |

[a]Abbreviations: NR = nanorod, NW = nanowire, *nc* = nanocrystals or nanocrystalline, PVK = poly(vinylcarbazole), TPD = N,N' - diphenyl-N,N' - bis(3-methylphenyl) - (1,1'-biphenyl) - 4,4'-diamine
[b]$V_{th} = E_{app}$ at the $EL$ emission threshold.
[c]$EQE_{max}$ = The maximum $EQE$.

## 1.2 Carrier Generation and Transport in M-S-M Structures

Electroluminescence is generated through the radiative recombination of free electrons and holes either within the material or at the interface between the material and the contact. So the density and distribution of these free electrons and holes would be the key factors for electroluminescence.

For a M-S-M structure, there are three important parts : a) the first metal-semiconductor (M-S) contact; b) the bulk part of the semiconductor material; c) the second M-S contact. These two M-S contacts would form two Schottky barriers on two sides. Upon a potential applied on the two metal contacts, electrons and holes will start to flow within the structure due to the electric force. The band energy diagram for a n-type M-S-M structure is showed in Figure 1.1. [56, 55, 9] (We are only interested in n-type semiconductor here since the material CdSe we study is a n-type semiconductor.)

For these two M-S contacts, free electrons are injected from the right contact which forms a reverse biased Schottky barrier with the middle semiconductor and holes are injected from left contact which forms a forward biased Schottky barrier with the middle semiconductor. As Firgure 1.1 shows, there are two barriers for electron flow at these two contacts: $\phi_{Bn}$ and $\phi_{in}$. $\phi_{in}$ is much smaller than $\phi_{Bn}$ and would become 0 when $E_{app}$ is big enough. So the limiting factor for electron flow is $\phi_{Bn}$ at the right Schottky barrier. For a n-type semiconductor, the carrier concentration of holes is much lower than the carrier concentration of electrons, so the contribution of holes to the current can be ignored. However, hole injection still plays an very important role here. When holes are injected from the left contact into the middle semiconductor, hole concentration would increase. This increase could amplify the probability of radiative recombination of free electrons and holes within a n-type semiconductor where hole concentration is very small compared to electron concentration. In

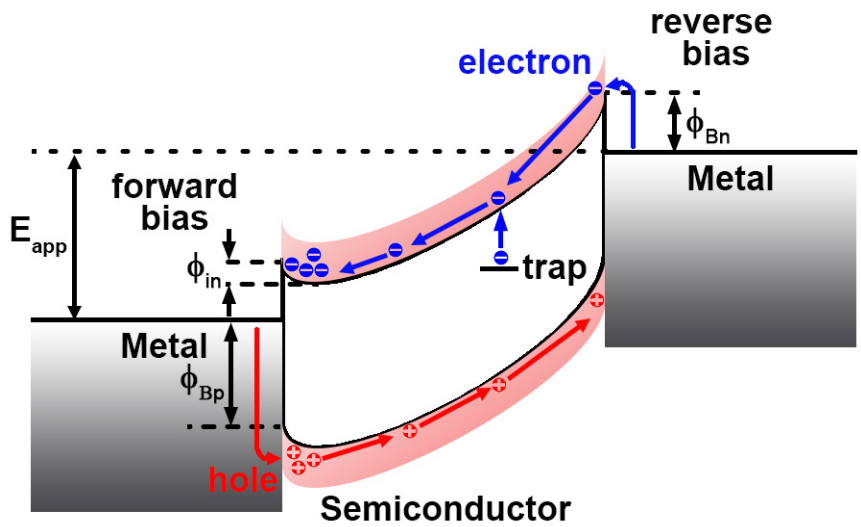


Figure 1.1: Band energy diagram for a M-S-M structure under an applied potential. $E_{app}$ is the applied potential, $\Phi_{Bn}$ is the Schottky barrier height for electrons, $\Phi_{Bp}$ is the Schottky barrier height for holes, $\Phi_{in}$ is barrier height caused by the build in potential for electrons which is equal to $V_{bi} - V_1$ where $V_{bi}$ is the build in potential and $V_1$ is the potential distributed on this M-S interface

summary, the limiting factor for total current or carrier injection at the two M-S contacts is the barrier height at the reverse biased Schottky barrier.

For the bulk part, free electrons could be generated from traps. Since the energy level of traps is lower than the conduction band, extra energy would need to be provided for electrons to jump from this barrier. Similar as Schottky emission, this process can be realized through thermal activation. Under electric field, the barrier height could be lowered and this thermal activation process could be enhanced. This is called Poole-Frenkel emission. [49, 9] Besides electron emission, electron transport also happens within the bulk part and there could be several different situations.

**Hopping Conduction.** With outside potential or electric field, electrons could hop from one trap site to another trap site due to the tunneling effect. It depends on the trap depth or the distance between the trap state and the bottom of conduction band, the distance

between two traps, and also the field strength.

**Space Charge Limited Conduction.** When free electrons are injected into intrinsic and low doped semiconductor, the electron flow could be affected a lot by space charges which make the electric field ununiform in the material. Space charge limited conduction (SCLC) is characterized by Child's law[7] or Mott-Gurney's law[33] which features $I \propto V^2$. For a M-S-M structure with SCLC, $I - V$ curve usually has three regions: 1) Ohmic like conduction region where $I - V$ curve is linear or $I \propto V$; 2) Child's law region which has $I \propto V^2$; 3) traps-filled-limit (TFL) region which has a enormously steep current rise. With $lnI - lnV$ curve, the slope would correspond to 1, 2, $> 2$ regions. [17, 26, 45, 35, 9]

**Grain-Boundary-Limited Conduction.** For a polycrystalline material, there are a lot of grain boundaries. When electrons flow to a grain boundary, it would experience a much higher resistivity than that in the grain. In terms of energy, the grain boundary function like an energy barrier and it would limit the electron flow. [43, 53] Under extra electric field, the barrier height could also be lowered like Poole Frenkel emission. So experimentally this process might not be able to be indentified out separately.

In summary, carrier injection and transportation in a n-type M-S-M structure is dominated by the electron injection and transportantion. This process could be limited by the contact or the bulk depending on the material properties and the device geometry. Through the shape of $I - V$ curve, we might be able to tell which part is the limiting factor.

# Chapter 2

# Electrodeposited, Transverse Nanowire Electroluminescent Junctions



## 2.1 Process Flow

*tn-ELJs* are prepared using a process (Figure 2.1) that provides for precise control of the width (± 5 nm) of the CdSe nanowire - which coincides with the electrical axis of the device - and the height (± 2 nm) the CdSe nanowire - which corresponds to the optical axis of the device. A second attribute of *tn-ELJs* is that the two metal-semiconductor junctions are both prepared by electrodeposition, thereby insuring electrically intimate contact between

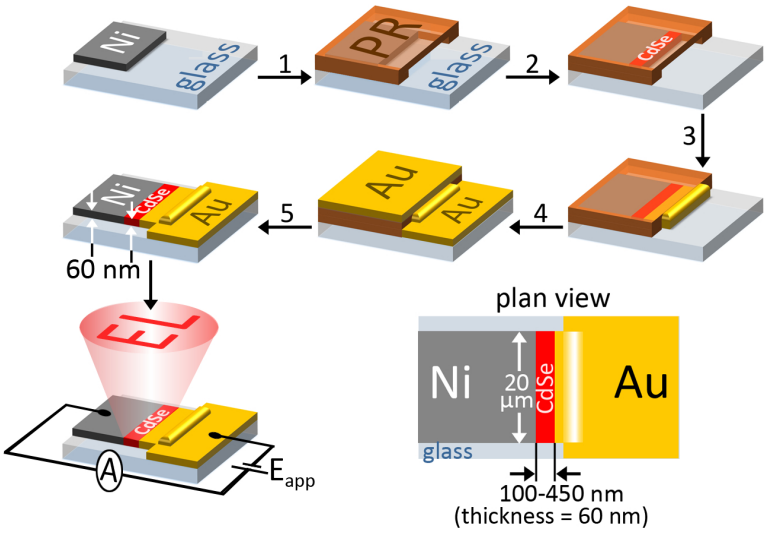


Figure 2.1: Simplified process flow for the fabrication of a single transverse nanowire electroluminescent junction (*tn-ELJ*). In Step 1, an evaporated nickel film on glass is patterned using photolithography. After spincoat of a photoresist (PR) layer and some additional processing, a horizontal trench is produced adjacent to the edge of the nickel film. This trench has dimensions of 60 nm (height), 20 $\mu$m (length) and 300 nm $\sim$ 1$\mu$m (depth). In Step 2, this patterned nickel edge is immersed in a plating solution and CdSe nanowires are electrodeposited within the trench using the nickel edges as working electrodes. The width of the CdSe nanowires is controlled by the electrodeposition conditions, which are identical for every nanowire. A gold electrical contact is then electrodeposited onto each CdSe nanowire. After the trench is filled with gold, the excess gold emerges from the trench forming a bump, as depicted in Step 3. In Step 4, a gold film is evaporated onto the entire surface of the device and then, in Step 5, the gold-coated photoresist layer is removed by lift-off. *tn-ELJ* devices produce *EL* light emission upon the application of a voltage bias to the nickel and gold contacts.

nickel and CdSe (Figure 2.1, step 2), and subsequently, CdSe and gold (Figure 2.1, step 3). Finally, in contrast to stacks of 2D films where the electrical and optical axes are coincident, the optical axis of the *tn-ELJ* is orthogonal to the electrical axis, allowing independent optimization of these dimensions for these two functions. The precision of *tn-ELJ* fabrication exposes the dominant influence of the *nc*-CdSe nanowire width, $w_{CdSe}$, on the two major metrics characterizing *EL* performance - the threshold for light emission, $V_{th}$, and the *EQE*.

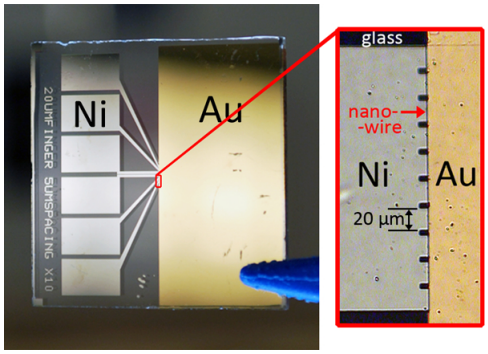


Figure 2.2: *tn-ELJ* device pictures. a) Photograph of 6 individual Ni-CdSe-Au *tn-ELJ* array devices on glass. The CdSe nanowires are vertically oriented along the left edge of the gold film. b) Photomicrograph of one of the six devices. Each device has ten individual nickel contacts to CdSe nanowires, and each is 20 $\mu$m in width.

## 2.2 Results and Discussion

### 2.2.1 Electrodeposition

*tn-ELJs* were prepared using a version of the lithographically patterned nanowire electrodeposition (LPNE) process (Figure 2.1) that we have previously described.[59, 32] The lithographically patterned nickel electrode that is employed for CdSe electrodeposition serves as one electrical contact to a CdSe nanowire, and the second gold electrode is electroplated at the CdSe surface (Figure 2.1). This process, carried out in parallel, provides a means for preparing a total of sixty pairs of nickel-gold electrodes in groups of ten, coupled with sixty nearly identical CdSe nanowires (Figure 2.2).

Uniformity of the CdSe nanowire width is achieved by electrodepositing the CdSe nanowire according to the reaction: $Cd^{2+} + H_2SeO_3 + 4H^+ + 6e^- \rightarrow CdSe(s) + 3H_2O$ under conditions of activation control. Here, this was accomplished using potentiostatic deposition at -0.60 V vs. SCE (Figure 2.3a). Electrodeposition current *versus* time transients (Figure 2.3b) show increasing current indicative of an increase in the wetted surface area of the nascent nanowire during electrodeposition. This increase in wetted surface area is likely the result of

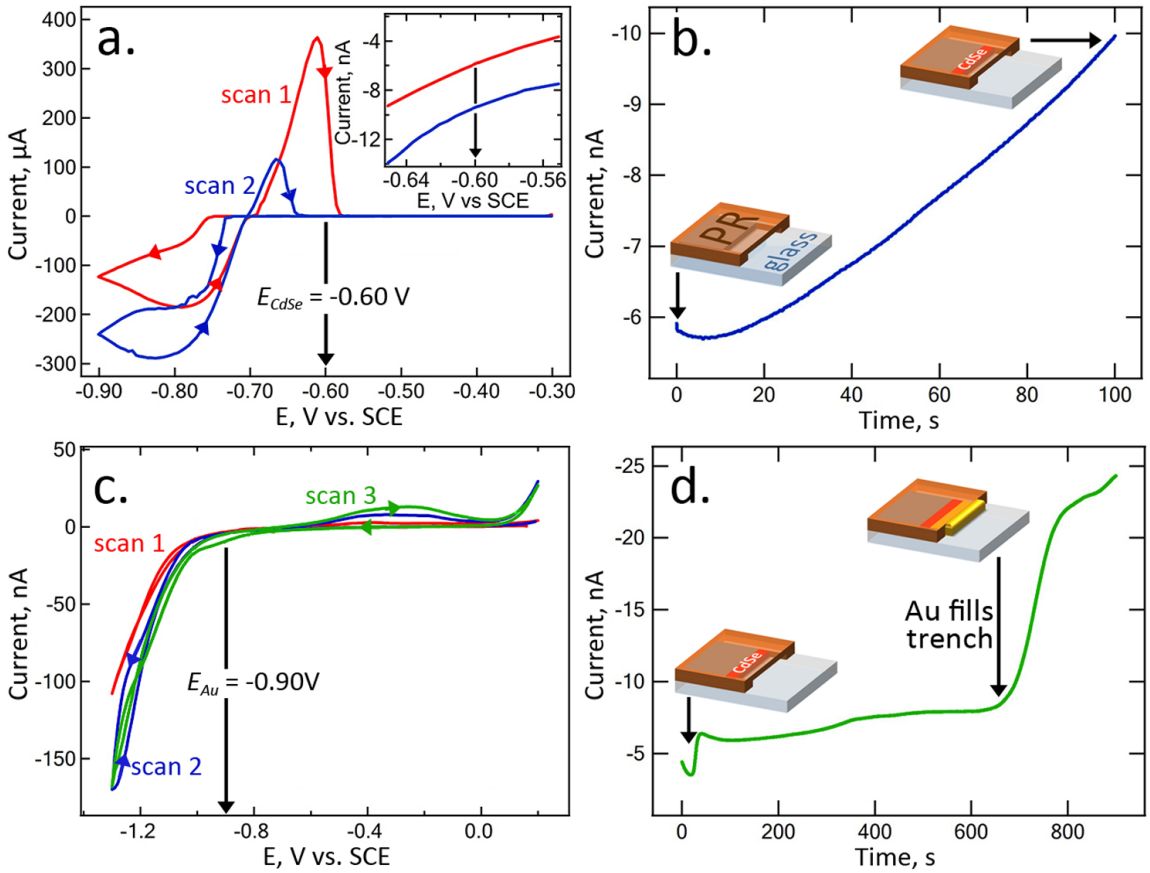


Figure 2.3: Electrodeposition of CdSe nanowires (a,b) and a gold contact (c,d). a) Cyclic voltammetry (50 mV/s) in the plating solution used for CdSe electrodeposition, containing 0.30 M $CdSO_4$, 0.70 mM $SeO_2$, and 0.25 M $H_2SO_4$ at pH 1-2. b) Current *versus* time transient for the potentiostatic growth at -0.60V of CdSe nanowires. CdSe nanowires with widths, $w_{CdSe}$, ranging from 102 nm to 448 nm were prepared by increasing the electrodeposition time from 20s to 100s. c) Cyclic voltammogram (50 mV/s) for a commercial gold plating solution acquired using the edges of CdSe nanowires. d) Current *versus* time transient for the potentiostatic growth at -0.90V of gold contacts at the CdSe nanowires. A rapid increase in current, starting at 650s, signals the filling of the photoresist trench.

the deposition of a porous CdSe deposit, since voids are visible in some of the SEM images presented below (Figure 2.4).

In each *tn-ELJ*, the lithographically patterned nickel electrode used to grow the CdSe nanowires serves as one electrical contact. The second contact, composed of gold, is prepared by electrodeposition directly onto the edge of the freshly-deposited CdSe nanowire. Again, this process is accomplished by the slow, activation-controlled deposition of gold (potentiostatic deposition at -0.90 V vs. SCE (Figure 2.3c)). A quasi-constant deposition current is observed during this process (Figure 2.3d) until the trench fills with gold (Figure 2.3d, 650s). At longer times, a rapid increase in the gold deposition current is observed resulting in the formation of a linear gold bump at the mouth of the trench, parallel to the CdSe nanowire (Figure 2.4a.) *tn-ELJ* device fabrication is completed by vapor depositing additional gold to facilitate the attachment of electrical leads.

### 2.2.2 SEM Characterization

SEM images of *tn-ELJ* Ni-CdSe-Au junctions (Figure 2.4) show that the width of the CdSe nanowire is conformal with respect to the nickel electrode (Figure 2.4a and inset) and directly proportional to the electrodeposition time. EDX elemental analysis (Figure 2.4c,e) shows the CdSe layer to be stoichiometric (Cd:Se=1.02±0.01) within the precision of this measurement. Five *tn-ELJ* with different $w_{CdSe}$ values, shown in Figure 2.4f-j, were investigated in this study. In recent prior work,[2, 60, 1, 25, 24] the properties of the *nc*-CdSe produced by an identical procedure have also been characterized by x-ray diffraction, Raman spectroscopy, and transmission electron microscopy. Electrodeposited *nc*-CdSe is crystalline, possesses a cubic crystal structure, and has a mean grain diameter of ≈5 nm.[2, 60, 1, 25, 24]

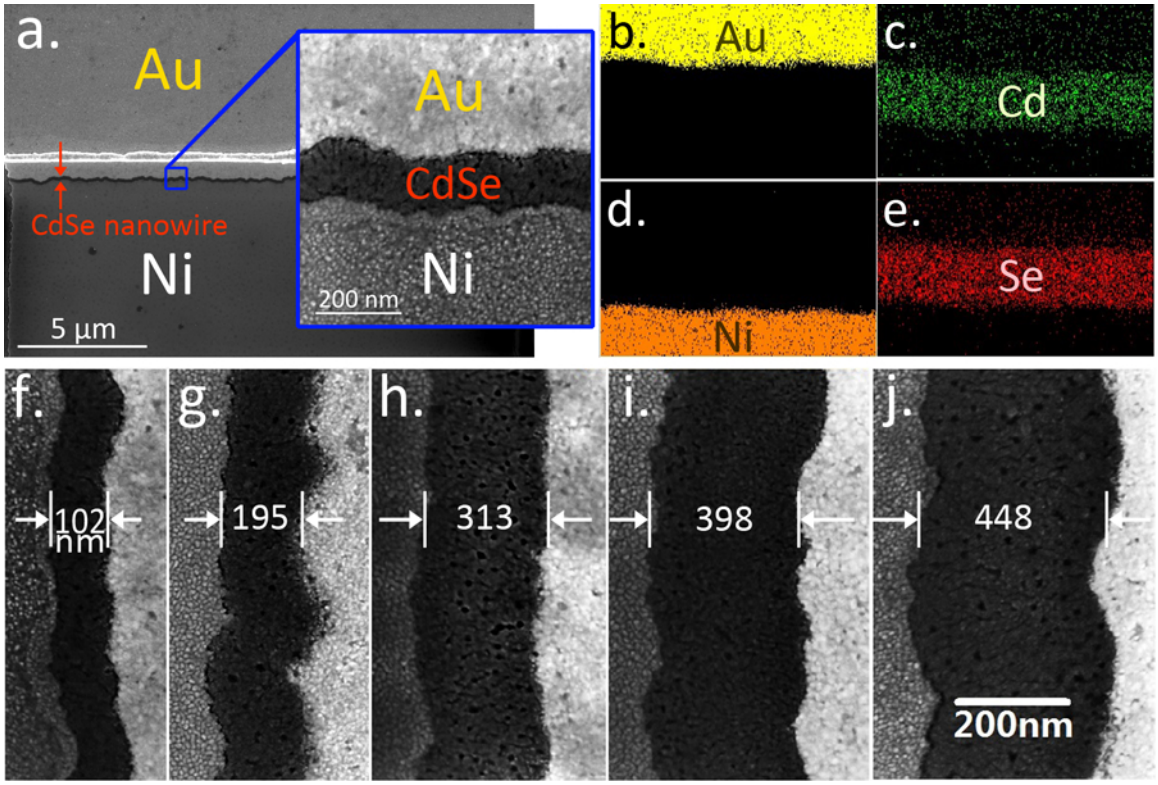


Figure 2.4: Scanning electron micrographs of *tn-ELJ* Ni-CdSe-Au junctions, all 60 nm in thickness. a) Low magnification image showing the horizontal CdSe nanowire, with top gold and bottom nickel electrodes. INSET: Higher magnification SEM image of the indicated region. b-e) EDX elemental maps of the junction region shown in the inset of (a) showing regions of Au (b), Cd (c), Ni (d), and Se (e). f-j) SEM images of five Ni-CdSe-Au *tn-ELJ* having $w_{CdSe}$ varying from 102 nm (f) to 448 nm (j).

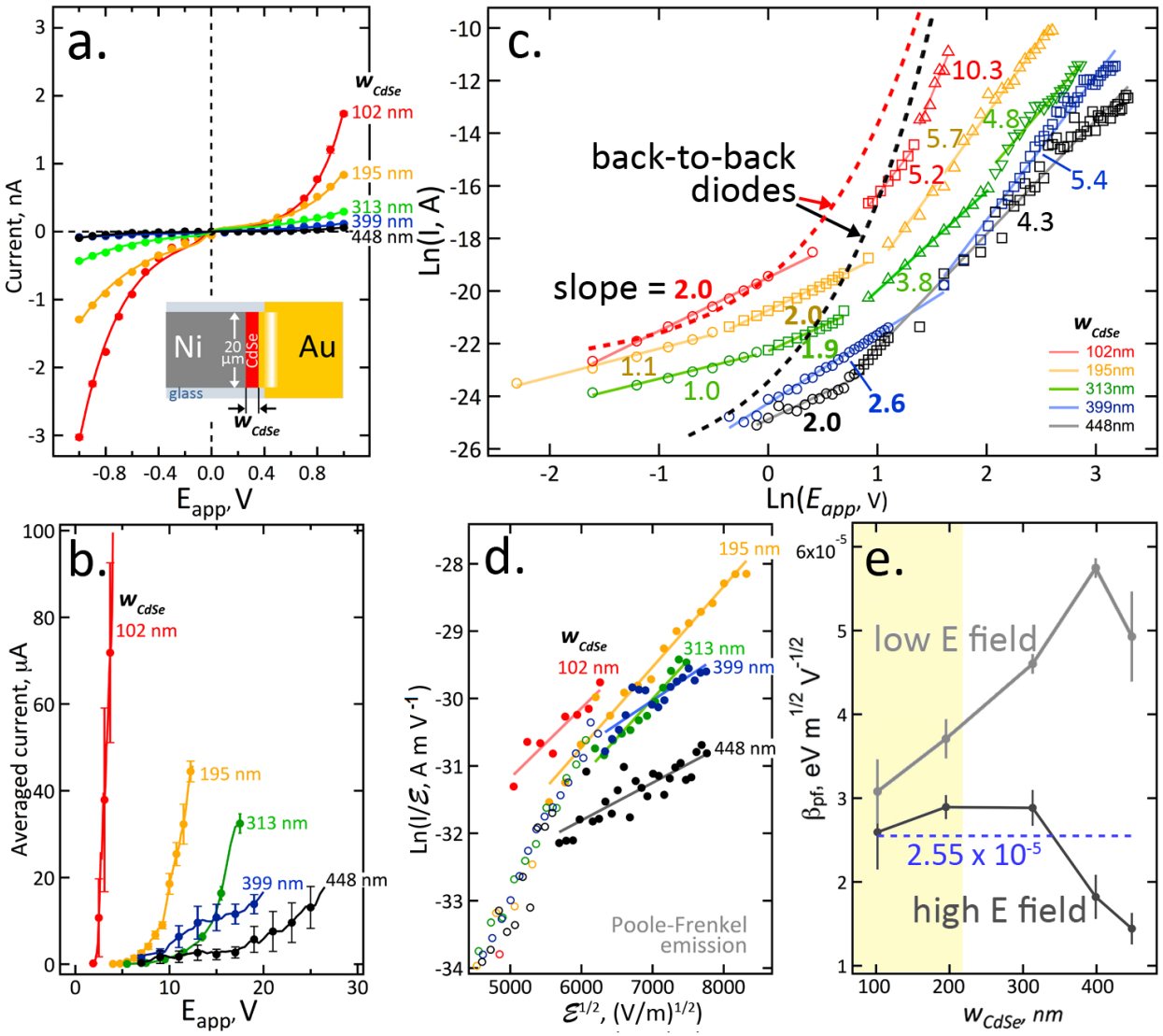


Figure 2.5: Electrical characterization of Ni-CdSe-Au *tn-ELJs*. a,b) Current *versus* voltage plots showing: a) low voltage ($E_{app} < 1.0$ V) and, b) high voltage region ($E_{app} > 1$ V in positive polarity only. c) Plot of Ln(I) *versus* Ln($E_{app}$) showing the slopes of linear regions of the $I - V$ data. The dashed red line and dashed black lines are the predictions of Eq. 1 for back-to-back Schottky barriers, using the parameters of Table 2.1 for $w_{CdSe} = 102$ nm and 448 nm, respectively. d) Plot of Ln(I/$\mathcal{E}$) *versus* $\mathcal{E}^{1/2}$ highlighting linear regions, consistent with possible Poole-Frenkel emission at high $\mathcal{E}$. e) Plot of Poole-Frenkel field lowering coefficient, $\beta_{pf}$, as a function of $w_{CdSe}$ for both high $\mathcal{E}$ (>3 × $10^7$ V/m) and low $\mathcal{E}$ regions.

Table 2.1: Fitting Parameters For Calculations of I-V Curves According to the Back-to-Back Schottky Barrier Model (Eq. 1)

| $w_{CdSe}$ (nm) | $A^{**a}$ (A cm$^{-2}$ K$^{-1}$) | ${\phi_{B1}}^b$ (eV) | ${\phi_{B2}}^c$ (eV) | ${n_1}^d$ | ${n_2}^e$ |
|---|---|---|---|---|---|
| 102 | 15.6 | 0.52 | 0.57 | 1.295 | 1.196 |
| 195 | 15.6 | 0.52 | 0.55 | 1.185 | 1.127 |
| 313 | 15.6 | 0.55 | 0.56 | 1.125 | 1.130 |
| 399 | 15.6 | 0.58 | 0.59 | 1.147 | 1.086 |
| 448 | 15.6 | 0.62 | 0.64 | 1.239 | 1.209 |

[a] $A^{**}$ = effective Richardson constant.[42]
[b] $\phi_{B1}$ = Schottky barrier height for Ni-CdSe contact.
[c] $\phi_{B2}$ = Schottky barrier height for Au-CdSe contact.
[d] $n_1$ = ideality factor for Ni-CdSe contact
[e] $n_2$ = ideality factor for Au-CdSe contact

### 2.2.3 Current Transport

Transport in metal-semiconductor-metal (M-S-M) junctions where both junctions are Schottky barriers was studied by Sze *et al.* in 1971[56] and subsequently by others.[39, 37, 8] With the application of a potential, $E_{app}$, the M-S-M has one forward biased Schottky barrier (with (+) polarity) and one reverse biased Schottky barrier ((−) polarity) and transport, predominantly by majority electrons, is controlled by the reverse-biased junction. Current *versus* $E_{app}$ (or *I-V*) curves are characterized by exponentially increasing current and, for identical metal contacts, are symmetrical about $E_{app} = 0$, conforming to the equation:[52, 8, 51]

$$J(V) = \frac{J_1 J_2 sinh(\frac{qV}{2KT})}{J_1 exp(\frac{qV}{2n_1KT}) + J_2 exp(-\frac{qV}{2n_2KT})} \tag{2.1}$$

Where $J_1$, for example, is given by:[55]

$$J_1 = A^{**}T^2 exp(-\frac{\phi_{B1}}{KT}) \tag{2.2}$$

and the equation for $J_2$ is analogous. Here $A^{**}$ is the effective Richardson constant. For CdSe, $A^{**}$ = 15.6 A cm$^{-2}$ K$^{-1}$).[42] $\phi_{B1}$ and $\phi_{B2}$ are the Schottky barrier heights of the Au-CdSe and Ni-CdSe contacts, respectively, and $n_1$ and $n_2$ are the two ideality factors for these junctions. Eq. 2.1 does an excellent job of fitting our experimental *I-V* curves for all five *tn-ELJs* and $w_{CdSe}$ values (Figure 5a). The fitting parameters required to produce these curves (Table 2.1) are also physically reasonable, involving the known Richardson constant and barrier heights in the range from 0.52 - 0.64 eV - close to those reported for macroscopic CdSe-Au Schottky barriers.[58] We conclude that for $|E_{app}| < 1.0$ V, *I-V* curves for *tn-ELJs* are well described by the back-to-back Schottky barrier model.[39, 37, 8]

For $|E_{app}| > 1.0$ V, however, the currents predicted by Eq. 2.1 are significantly higher than those observed experimentally for *tn-ELJs*. For example, using the parameters of Table 2.1, dashed lines in Figure 2.5c show the predicted *I-V* behavior for the 102 nm (red dashed line) and the 448 nm (black dashed line) *tn-ELJ*s. A comparison of the dashed curves with the experimental data points of the same color shows that the disparity between them increases with increasing $E_{app}$. This disparity is explained by the presence of a highly resistive CdSe layer in the *tn-ELJs*, sandwiched between the two Schottky barriers. Based upon the analysis of these currents described below, we conclude that transport through a *tn-ELJ* is not limited by transport at one or both of the Schottky barriers, but by processes occurring in the bulk of the CdSe, even though this "bulk" is nanoscopic in both length (≈100-450 nm) and thickness (60 nm).

Information on the transport mechanisms operating within the CdSe can be obtained by analyzing the $E_{app}$ dependance of the current. Space charge limited conduction (SCLC) has previously been proposed to model the *I-V* behavior of Au-CdSe-Au junctions.[38] SCLC conforms to the Mott-Gurney Eq.:[33]

$$J = \frac{9\epsilon_s \mu (E_{app})^2}{8d^3} \tag{2.3}$$

where $J$ is the current density (A/m$^2$), $\mu$ is the carrier mobility (m$^2$/(V·s)), $\epsilon_s = = 7.82$ x $10^{-11}$ F/m for CdSe, and $d = w_{CdSe}$[33] Eq. 2.3 predicts that Ln($I$) *versus* Ln($E_{app}$) will have a slope of 2.0, and this behavior is observed for four of the five of the CdSe thicknesses (Figure 2.5c); $w_{CdSe} = 399$ nm instead shows a slope of 2.6. In this potential regime, SCLC is likely the dominant mechanism of charge transport. At lower $E_{app}$, a slope of 1.0, indicative of ohmic conduction, is seen for several $w_{CdSe}$ ($w_{CdSe} = 195$ and 313 nm) . Slopes larger than 2.0 are observed for all devices at $E_{app} > 10$V. As previously described,[35, 4, 47] slopes exceeding 2.0 signal that the SCLC current is augmented by other transport mechanisms such as P-F emission or Schottky emission.

P-F emission conforms to Eq. 2.4 while, as already indicated, Schottky emission is modeled by Eq. 2.1:[49, 50, 55]

$$J = J_0 \, exp\left(\frac{\beta_{pf}\mathcal{E}^{1/2}}{kT}\right) \tag{2.4}$$

where $\beta_{pf}$ is the P-F field-lowering coefficient and $\mathcal{E}$ is the magnitude of the electric field ($E_{app}/d$).[50, 55] These two mechanisms both predict linear $Ln(I/\mathcal{E})$ *versus* $\mathcal{E}^{1/2}$, which we

Table 2.2: Discrete Slopes of Ln($I$) *versus* Ln($E_{app}$) Plots Observed at Progressively Higher $E_{app}$

| $w_{CdSe}$ (nm) | Slope 1 | Slope 2 | Slope 3 | Slope 4 |
|---|---|---|---|---|
| 102 | – | 2.03 (±0.05) | 5.2 (±0.2) | 10 (±1) |
| 195 | 1.1 (±0.1) | 2.00(±0.05) | 5.7 (±0.1) | – |
| 313 | 1.03 (±0.06) | 1.9 (±0.1) | 3.77 (±0.07) | 4.8 (±0.2) |
| 399 | – | 2.63 (±0.05) | 5.5 (±0.1) | – |
| 448 | – | 2.0 (±0.2) | 4.33 (±0.07) | – |

observe at high values of $\mathcal{E} > 3 \times 10^7$ V/m for all five devices (Figure 2.5d).

From the slope of these plots, an experimental value of $\beta_{PF}$ can be calculated and compared with the theoretically expected value for CdSe of 2.55 $\times$ $10^{-5}$ $eVm^{-1/2}$ $V^{1/2}$, indicated by the horizontal blue dashed line in Figure 2.5d. In the high $\mathcal{E}$ region $> 3 \times 10^7$ V/m, we measure $\beta_{pf}$ values in the range from 1.5 - 2.9 $\times$ $10^{-5}$ eV m$^{1/2}$ V$^{-1/2}$ - close to that expected for Poole-Frenkel emission in CdSe (Figure 2.5e). The best agreement is seen for the thinnest *tn-ELJs* ($w_{CdSe}$ = 102 and 195 nm) where $\beta_{pf}$ values are in the range from 2.6-2.9 $\times$ $10^{-5}$ eV m$^{1/2}$ V$^{-1/2}$. Much larger values of $\beta_{pf}$ are seen in the low $\mathcal{E}$ region $< 2 \times 10^7$ V/m where we believe that SCLC, not Poole-Frenkel or Schottky emission, is the dominant mechanism of charge transport. We interpret a high level of agreement of the experimental $\beta_{pf}$ value with the theoretical value to suggest the likely prevalence of P-F emission, as opposed to Schottky emission, in *tn-ELJs* at high $\mathcal{E}$.

To summarize these observations, our analysis of *tn-ELJs* reveals the operation of up to three discrete charge transport mechanisms in parallel - ohmic conduction, SCLC, and (likely) P-F emission - with increasing importance of SCLC and P-F emission as $E_{app}$ increases. The values of these discrete slopes (see in the plot of Figure 2.5c), which delineate voltage intervals in which particular mechanisms are operating, are tabulated in Table 2.2.

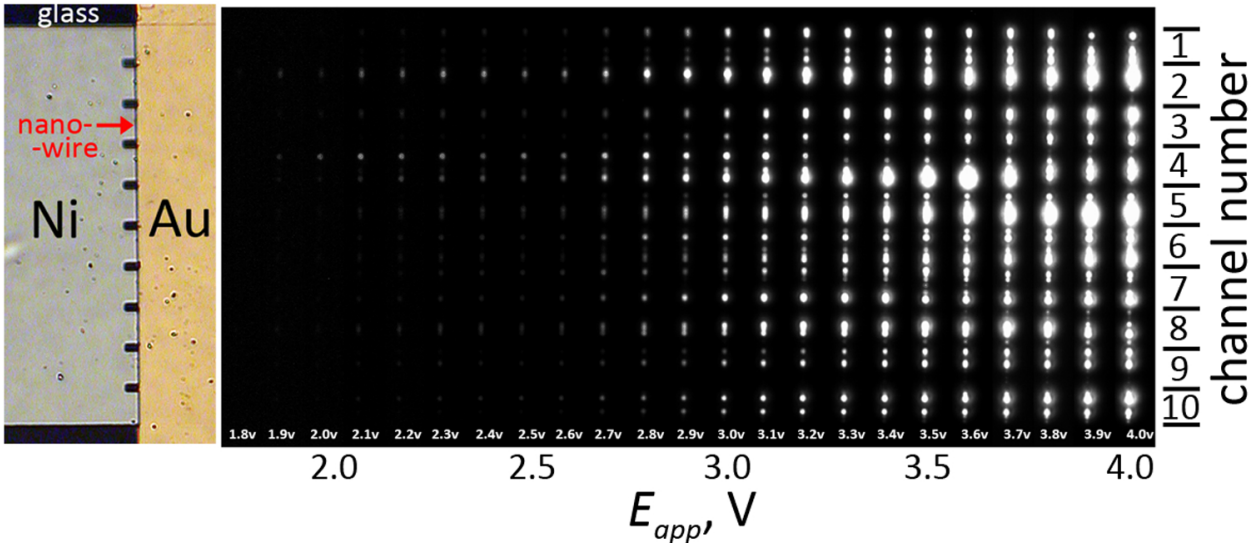


Figure 2.6: Optical micrograph of $EL$ emission as a function of $E_{app}$ for a ten-element *tn-ELJs* with $w_{CdSe}$ = 102 nm. At left is shown an optical micrograph of the ten electrode array, showing the vertical orientation of the CdSe nanowire and the position of the nickel contacts.

### 2.2.4 Electroluminescence Intensity and External Quantum Efficiency

$EL$ emission from ten-element arrays of Ni-CdSe-Au *tn-ELJs* (Figure 2.6) was imaged as a function of $E_{app}$ using an inverted optical microscope (Figure 2.9). For the $w_{CdSe}$ = 102 nm device, all ten channels produce $EL$ at $E_{app}$ = 3-4V, but $EL$ emission intensity increases with $E_{app}$ and is non-uniformly distributed within each channel and between different channels (Figure 2.6) - a characteristic feature of $EL$ in these systems that we discuss below. The properties this $EL$ emission depended sensitively on the width of the CdSe emitter layer, $w_{CdSe}$ (for a constant 60 nm height of this emitter layer, Figure 2.7a). For example, the voltage threshold for $EL$ emission, $V_{th}$, increases from 2V to 7V in direct proportion to $w_{CdSe}$ (Figure 2.7a,b). This trend is also evident in prior work involving CdSe $EL$ emitting device structures where the spacing of electrodes has been varied (Table 1.1), and it derives in part from the ohmic resistance imposed by the emitter layer. The lowest values for $V_{th}$ are

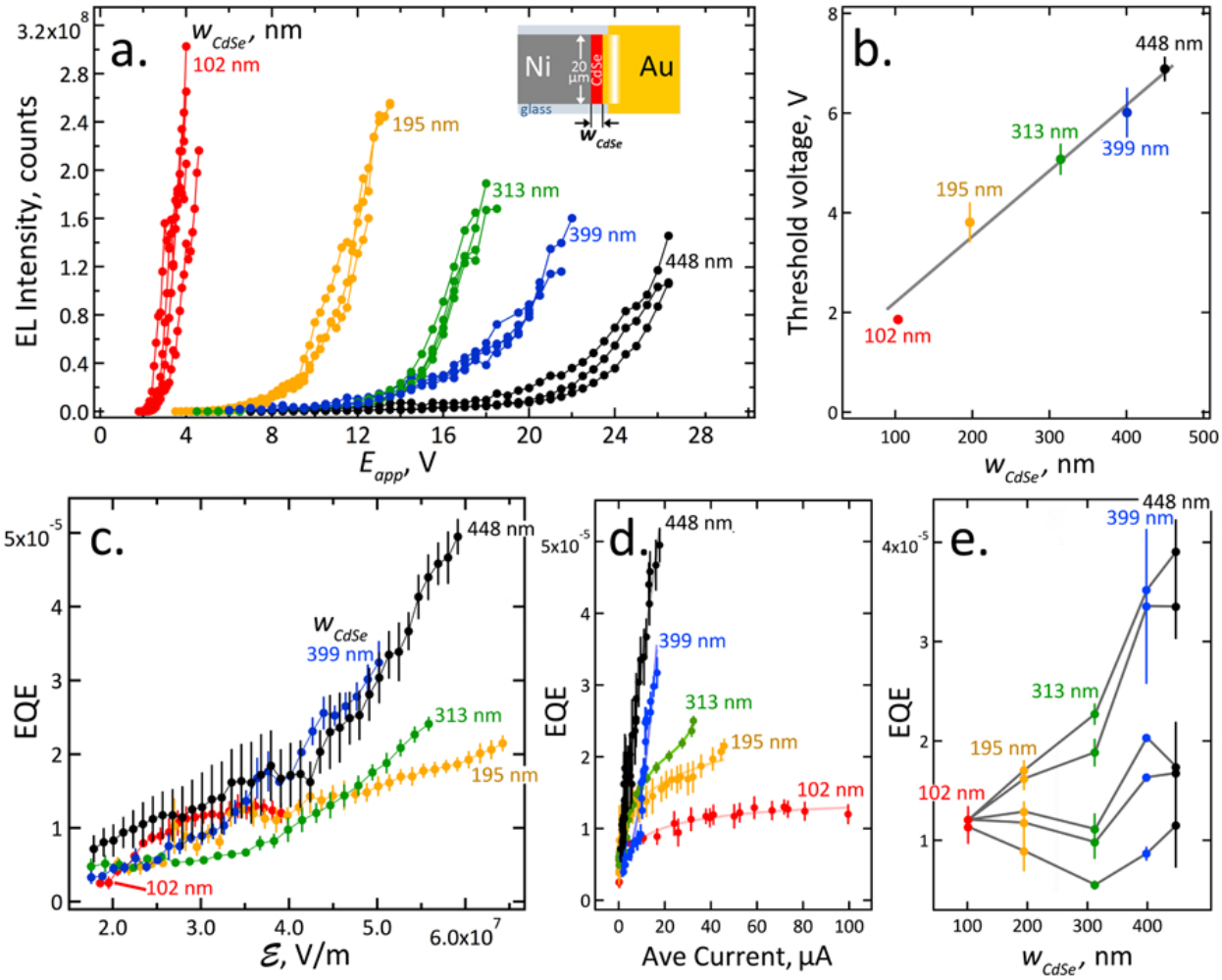


Figure 2.7: Optical characterization of Ni-CdSe-Au *tn-ELJs*. a) *EL* intensity *versus* $E_{app}$ for five widths of devices described in Figure 2.5. Error bars represent $\pm 1\sigma$ for $n$ devices as follows: $n = 3$ ($w_{CdSe} = 102$ nm), $n = 3$ (195 nm), $n = 4$ (313 nm), $n = 4$ (399 nm), and $n = 3$ (448 nm). b) Threshold voltage, $V_{th}$, *versus* $w_{CdSe}$. Here, $V_{th}$ is estimated as the lowest voltage at which *EL* emission is observed above background. c) External quantum efficiency (EQE) *versus* electric field, $\mathcal{E}$ for the five devices described in Figure 2.5. d) *EQE* *versus* average device current. e) *EQE* for the five devices described in Figure 2.5, each corresponding to five discrete $\mathcal{E}$ values: 2.85, 3.90, 4.15, 5.15, 5.50 ($\times 10^7$ V/m).

those where the narrowest electrode spacings were used. For example, Gudiksen *et al.*[18] reported a $V_{th}$ of 1.7V for $EL$ emission from transistors with electrode spacings of 30 nm. $EL$ from gold nanogaps that are 100-200 nm in width and filled with electrodeposited CdSe[60] are characterized by $V_{th}$ = 1.5 - 1.9V. It should be noted that even lower values of $V_{th}$ have been demonstrated in cases where hole and electron transporting layers have been added on either side of the CdSe emitted layer, irrespective of the electrode spacing.[30, 27, 54, 65, 46]

*tn-ELJs* with narrow CdSe emitters are also capable of brighter $EL$ emission. For example, the maximum $EL$ intensity produced at $w_{CdSe}$ = 102 nm using 3V is twice as high as the maximum $EL$ intensity measured for the 448 nm *tn-ELJs* at 26V (Figure 2.7a). But the quantum efficiency of $EL$ emission is actually inversely correlated with $w_{CdSe}$. In the plot of external quantum yield (EQE) *versus* the electric field, $\mathcal{E}$ (Figure 2.7c), devices with all five values of $w_{CdSe}$ show similar $EQE$ values at low $\mathcal{E}$ of $\approx 2 \times 10^7$ V/m. But for higher fields of up to $6 \times 10^7$ V/m, $EQE$ is preferentially increased for the widest emitter layers ($w_{CdSe}$ = 313, 399, and 448 nm). At high fields, for example, the 448 nm *tn-ELJs* produces an $EQE$ ($\approx 5 \times 10^{-5}$) that is five times as high as the maximum $EQE$ measured for the 102 nm *tn-ELJs*. This $EQE$ is amongst the largest measured for CdSe $EL$ devices that do not have dedicated hole and/or electron injection layers (Table 1.1).

A plot of $EQE$ *versus* current (Figure 2.7d) shows that, in general, $EQE$ increases monotonically with increasing current. The slope of this increase is correlated with $w_{CdSe}$. The exception to this rule involves the narrowest emitter layer, $w_{CdSe}$ = 102 nm, where the $EQE$ first increases, and then reaches a plateau at a maximum $EQE$ of $\approx 1.2 \times 10^{-5}$. Wider CdSe layers show more steeply sloping $EQE$ *versus* current behavior, and larger $EQE_{max}$ as current is increased, but the maximum attainable current and therefore $EQE$ in wide CdSe emitter layers are both limited (Figure 2.7d).

In Figure 2.7e, the $EQE$ is plotted for *tn-ELJs* as a function of $w_{CdSe}$ for five discrete $\mathcal{E}$ values. This plot highlights the fact that wide CdSe emitter layers produce elevated $EQE$

only at high fields, $\mathcal{E} > 5 \times 10^7$ V/m. At lower $\mathcal{E}$ values, $EQE$ for *tn-ELJs* with five $w_{CdSe}$ are within a factor of two of each other (Figure 2.7e).

### 2.2.5 Electroluminescence Spectra and Mechanisms

A typical $EL$ spectrum for a *tn-ELJs* (Figure 2.8a) shows a broad emission envelope spanning the wavelength range from 500 nm to 1000 nm. A photoluminescence (PL, $\lambda_{ex} = 532$ nm) spectrum for electrodeposited *nc*-CdSe is much narrower, and centered at the 725 nm bandgap, $E_{bg}$, of CdSe (Figure 2.8). This dramatic broadening of the spectral output in $EL$ as compared with $PL$ has been observed in many previous studies involving a range of materials.[3, 15, 28, 14, 18, 46] A second characteristic feature of $EL$ emission in *tn-ELJs*, already seen in Figure 2.6, is that the $EL$ produced within a 20 $\mu$m wide element consists of a series of sub-micron point emitters - even at high $E_{app}$. This is apparent in the images and plots of Figure 2.8b that show emission from a $w_{CdSe} = 195$ nm *tn-ELJ* at $E_{app}$ from 4.5 V to 13.5 V. One possible reason for localized light emission is modulation of the electric field along the axis of each CdSe nanowire, caused by its width nonuniformity. In this case, local constrictions in width would correlate with a locally higher $\mathcal{E}$ and enhanced $EL$ emission. The number and total area of the light emitting regions increases with $E_{app}$. The spectrum of Figure 2.8a was acquired for a device consisting of ten *tn-ELJs*, and therefore contains many point emitters. Spectra for single point emitters could not be acquired in this study, but there is evidence that the broad emission seen in Figure 2.8a is produced by each point emitter and is not the sum of many narrower emission spectrs produced by an ensemble of point emitters. The evidence takes the form of the potential dependence (Figure 2.8a). At low $E_{app}$ values ($\approx$4 V), just a handful of point emitters are observed and the total $EL$ intensity is very low, but the spectral width of the $EL$ emission is similar to that seen at higher $E_{app}$ values, although emission is somewhat red-shifted. This observation suggests that each micron-scale emitter produces a broad spectrum and that the spectral width seen

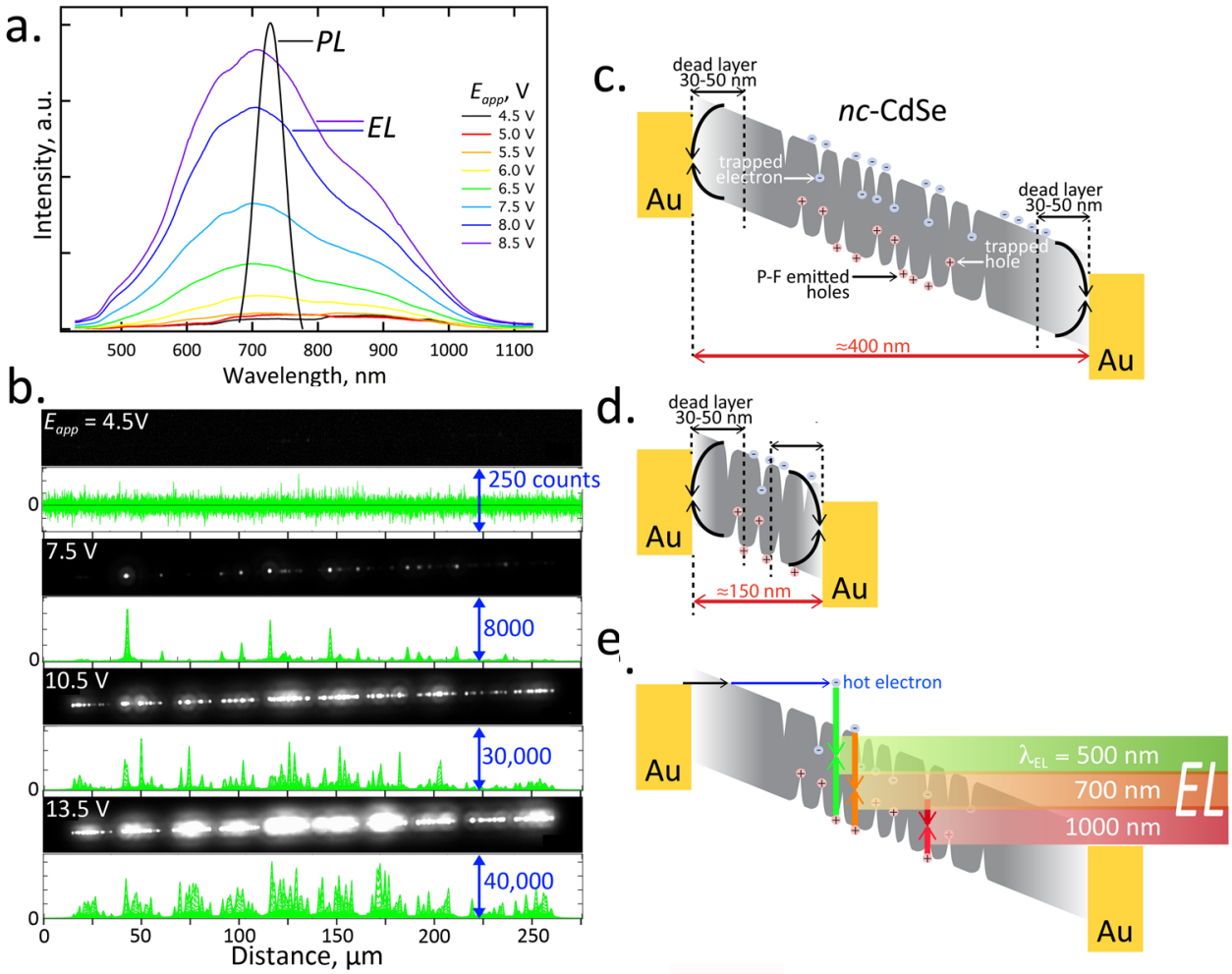


Figure 2.8: Spectra and proposed mechanism for $EL$ emission. a) $EL$ spectra as a function of $E_{app}$ for a ten-element *tn-ELJs* with $w_{CdSe} = 102$ nm. PL spectrum acquired with excitation at $\lambda_{ex} = 532$ nm. b) Micrographs and intensity plots for a $w_{CdSe} = 195$ nm *tn-ELJs* at four $E_{app} = 4.5$V - 13.5V. EL emission consists of a series of sub-micron point emitters that coalesce at high $E_{app}$. c) Schematic energy level diagram for a wide ($w_{CdSe} = 400$ nm) *nc*-CdSe emitter layer illustrating the presence of deep trap states for electrons and holes, and the presence of a dead layer in which $e^-/h^+$ recombination is nonradiative. d) Same diagram as in (c) except illustrating a narrow ($w_{CdSe} = 150$ nm) *nc*-CdSe emitter layer, e) Processes contributing to broad-band $EL$ emission including hot electron-hole recombination ($h\nu > E_{bg}$, green), band-edge emission ($h\nu \approx E_{bg}$, orange), and free hole-trapped electron recombination ($h\nu < E_{bg}$, red).

for many emitters (e.g., Figure 2.8a) is not a function of the number of emitters, with each producing a much narrower emission envelope.

A schematic band diagram (Figure 2.8c-e) illustrates the salient features of $EL$ emission in these nickel-(*nc*-CdSe)-gold *tn-ELJs*. The observed reduction in $EQE$ with decreasing $w_{CdSe}$ (Figure 2.7d,e) suggests the presence of "dead layers" adjacent to the metal contacts within which $EL$ is quenched. This phenomenon has been described previously in connection with $EL$ in thin-film M-S-M devices,[13, 34] but the mechanism responsible for dead layers remains unresolved. One possible mechanism accounting for a dead layer adjacent to metal contacts is the physical diffusion/migration of electrons and/or holes to these metal contacts and their subsequent radiationless recombination. In this case, the thickness of the dead layers should approximate the minority carrier diffusion length, estimated to be 30-50 nm based upon our prior measurements of carrier mobilities [2] and minority carrier lifetimes[25] in electrodeposited *nc*-CdSe. A second possibility, also suggested by others,[36] is that radiationless recombination near a contact is a symptom of poorer CdSe quality, in terms of impurities and crystallinity. Further work will be required to elucidate this mechanism.

Also as depicted in Figure 2.8c-e, the *nc*-CdSe emitter contains deep traps for both electrons and holes, associated mainly with disorder and inpurities at grain boundaries. As $E_{app}$ is increased, $\mathcal{E}$ exceeds the threshold for P-F emission ($> 5 \times 10^7$ V/m) which triggers the release by field-ionization of trapped holes. Field-emitted, mobile holes rapidly and radiatively recombine with electrons to produce $EL$. The broad spectral envelope for $EL$ emission seen in Figure 2.8a is accounted for by the operation of three processes in parallel (Figure 2.8e): i) hot electron-hole recombination ($h\nu > E_{bg}$, green), ii) band-edge emission ($h\nu \approx E_{bg}$, orange), and, iii) free hole-trapped electron recombination ($h\nu < E_{bg}$, red). But although $EL$ emission that is red-shifted from $E_{bg}$ is likely caused by trapped carriers, it remains unclear (also in other studies) why the electron and hole traps leading to red-shifted emission in $EL$ are preferentially populated in $EL$ relative to $PL$.

### 2.2.6 Conclusion

In conclusion, we describe a discovery platform that consists of arrays of transverse nanowire light emitting nanojunctions or *tn-ELJs*. These device arrays have the potential to advance our understanding of $EL$ in electrodeposited materials - in this case, arrays of nickel-($nc$-CdSe)-gold *tn-ELJs*. These *tn-ELJs* exhibit highly reproducible, and tunable, properties for $EL$ light emission that are strongly influenced by the width of the CdSe emitter layer along the electrical axis, $w_{CdSe}$. Transport in *tn-ELJs* involves a progression of three mechanisms as $E_{app}$ is increased - ohmic conduction, space-charge limited conduction, and Poole-Frenkel (P-F) emission. The voltage threshold for light emission, ranging from 2 V to 7 V, is directly proportional to $w_{CdSe}$ from 100 nm to 450 nm. The external quantum efficiency ($EQE$) of the observed $EL$ increases for all *tn-ELJs* with the applied electric field, suggesting that P-F emission of mobile holes into the valance band is rate-limiting. Finally, the maximum external quantum efficiency ($EQE_{max}$) also increases monotonically with $w_{CdSe}$, up to $5 \times 10^{-5}$ for $w_{CdSe} = 450$ nm. These observations are consistent with a mechanism of $EL$ light emission involving the P-F emission of holes in the valence band of the electrodeposited $nc$-CdSe nanowire, with subsequent radiative recombination with electrons that are both injected above the conduction band-edge (hot electrons), and others that are trapped, leading to a broad spectral bandwidth for the emission process. Working in opposition to this process is nonradiative electron-hole recombination near (within 30-50 nm) the metal electrical contacts, leading to higher $EQE$ in wide CdSe emitters.

The maximum EQE obtained here of $5 \times 10^{-5}$ is low, but comparable or better than in previous studies where the same M-S-M architecture has been studied (Table 1.1). In future work, the influence of dedicated hole and electron injecting and transporting layers adjacent to the CdSe emitter layer will be evaluated as a means for obtaining higher $EL$ quantum efficiencies.[48, 54]

## 2.3 Methods

### 2.3.1 Device Fabrication

CdSe light emitting devices were fabricated using the LPNE method in combination with several additional photolithography steps (Figure 2.1). First, a 60 nm thick layer of nickel was thermally evaporated on a precleaned soda lime glass slide (2.5 cm $\times$ 2.5 cm $\times$ 1 mm). Then a layer of photoresist (PR, Shipley, S1808) was spin-coated (2500 rpm, 80 s) onto the nickel surface, followed by a soft-bake at (90°C) for 30 min. The PR-coated nickel was then covered with a contact mask, exposed to UV light, and the exposed PR was developed for 20 s (Microposit, MF-319), rinsed with water (Millipore MilliQ, $\rho > 18$ M$\Omega\cdot$ cm), and air dried. The freshly exposed nickel layer was then removed using nickel etchant (Alfa Aesar) for 2 min, resulting in six parallel 10-finger patterns consisting of 20 $\mu$m wide Ni-CdSe-Au *tn-ELJs* spaced by 5 $\mu$m (Figure 2.2). The photoresist layer was then removed with acetone and a second layer of photoresist (Shipley, S1808) was spin-coated and photolithographically patterned. Exposed nickel was over-etched in 0.80 M nitric acid for 6 8 min to create a horizontal trench with a width of 300 nm $\sim$ 1 $\mu$m at the end of each nickel finger.

CdSe nanowires were electrodeposited into these trenches potentiostatically at -0.60 V *versus* saturated calomel electrode (SCE) in an unstirred, room temperature, aqueous plating solution consisting of 0.30M $CdSO_4$, 0.70mM $SeO_2$, and 0.25 M $H_2SO_4$ at pH 1-2. (Caution: both $CdSO_4$ and $SeO_2$ are highly toxic). Gold contacts were then electrodeposited onto the solution-exposed edge of the CdSe nanowire potentiostatically at -0.90 V *versus* SCE using a Clean Earth Inc. gold plating solution. Gold deposition was continued until the gold emerged from the trench, as signaled by an increase in the electrodeposition current (Figure 2.3d). All electrodeposition operations were carried out using a Gamry Series G 300 potentiostat in conjunction with a one compartment three-electrode electrochemical cell with SCE as the reference electrode and platinum foil as the counter electrode. After gold electrodeposition,

a layer of gold was thermally evaporated to form a connection with the electrodeposited gold contact, facilitating the attachment of wire contacts. The PVD-deposited gold on the photoresist coated portion of the device was removed by lift-off.

### 2.3.2 Structural Characterization

Scanning electron microscopy (SEM) images were acquired using a FEI Magellan 400 XHR system at an accelerating voltage of 1 or 8 keV without metal or carbon coating. Energy-dispersive X-ray spectroscopy (EDS) images were also acquired using this instrument which is equipped with a 80 $mm^2$ silicon drift X-ray detector (Oxford Instruments, with Aztec software).

### 2.3.3 Electroluminescence and Photoluminescence

EL images as a function of bias were acquired using an inverted microscope (Olympus, IX71) equipped with a 40× objective lens (Olympus, LUCPlanFLN $40 \times 0.60$) and a CMOS camera (Andor, Neo) as Figure 2.9 shows. Electrical measurements during $EL$ emission were accomplished using a sourcemeter (Keithley 2400) controlled by LabVIEW software. EQE was calculated using the number of photons out of *tn-ELJs* devices devided by the number of electrons flowing through the material per second. Cmos sensitivity and geomtry loss was factored into calculation. $EL$ spectra were obtained using a spectrometer (Andor, Shamrock SR-500i-D2) equiped with a 300 l/mm grating blazed at 760nm and a CCD camera (Andor, Newton). All the $EL$ measurements were carried out under cooling condition using a Peltier cooling device (Custom Thermoelectric, 19012-5L31-06CQQ-X) in nitrogen environment(to avoid water condensation or frost). PL spectra were acquired using a SpectraPro 2300i spectrometer (Princeton Instruments, Acton) excited by a 532nm laser.

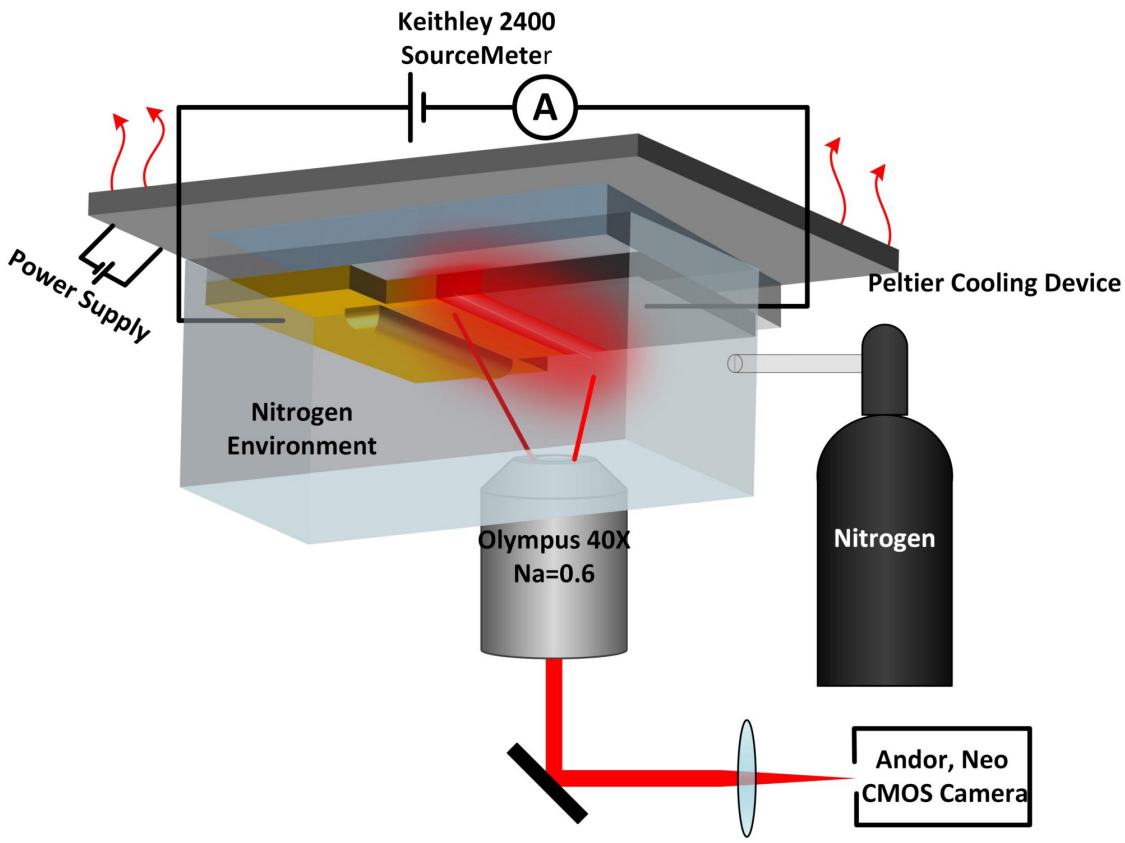


Figure 2.9: EL measurement set-up. The *tn-LEJs* was glued on a $1inch \times 3inches$ glass slide then glued on a peltier cooling device using the copper tape. The peltier was used to remove the heat generated during EL measurement. The *tn-LEJs* was connected to a Keithley 2400 sourcemeter, and then the whole device was placed on an inverted microscope stage. The device along with the objective lens were wrapped with regular food wrap to create a sealed environment. The food wrap was then pierced through by a small glass pipe connected with a nitrogen tank. A nitrogen environment was created during EL measurenment to avoid water condensation or frost.

# Bibliography


[1] Talin Ayvazian, Wytze E. van der Veer, Wendong Xing, Wenbo Yan, and Reginald M. Penner. Electroluminescent, polycrystalline cadmium selenide nanowire arrays. *ACS Nano*, 7(10):9469–9479, 2013.

[2] Talin Ayvazian, Wendong Xing, Wenbo Yan, and Reginald M Penner. Field-effect transistors from lithographically patterned cadmium selenide nanowire arrays. *ACS Appl. Mater. Interfaces*, 4(9):4445–4452, 2012.

[3] Jiming Bao, Mariano A. Zimmler, Federico Capasso, Xiaowei Wang, and Z. F. Ren. Broadband zno single-nanowire light-emitting diode. *Nano Lett.*, 6(8):1719–1722, AUG 9 2006.

[4] DF Barbe. Space-charge-limited current enhanced by frenkel effect. *J. Phys. D Appl. Phys.*, 4(11):1812, 1971.

[5] A-L Bavencove, G. Tourbot, J. Garcia, Y. Desieres, P. Gilet, F. Levy, B. Andre, B. Gayral, B. Daudin, and Le Si Dang. Submicrometre resolved optical characterization of green nanowire-based light emitting diodes. *Nanotechnology*, 22(34):345705 (9 pp), AUG 26 2011.

[6] Chih-Yen Chen, Guang Zhu, Youfan Hu, Jeng-Wei Yu, Jinghui Song, Kai-Yuan Cheng, Lung-Han Peng, Li-Jen Chou, and Zhong Lin Wang. Gallium nitride nanowire based nanogenerators and light-emitting diodes. *ACS Nano*, 6(6):5687–5692, JUN 2012.

[7] C. D. Child. Discharge from hot cao. *Phys. Rev.*, 32(5):492–511, may 1911.

[8] Adenilson J Chiquito, Cleber A Amorim, Olivia M Berengue, Luana S Araujo, Eric P Bernardo, and Edson R Leite. Back-to-back schottky diodes: the generalization of the diode theory in analysis and extraction of electrical parameters of nanodevices. *J. Phys.-Condens. Mat.*, 24(22):225303, 2012.

[9] Fu-Chien Chiu. A review on conduction mechanisms in dielectric films. *Adv. Mater. Sci. Eng.*, 2014:1–18, 2014.

[10] Seth Coe, Wing-Keung Woo, Moungi Bawendi, and Vladimir Bulović. Electroluminescence from single monolayers of nanocrystals in molecular organic devices. *Nature*, 420(6917):800–803, 2002.

[11] VL Colvin, MC Schlamp, and AP Alivisatos. Light-emitting diodes made from cadmium selenide nanocrystals and a semiconducting polymer. *Nature*, 370(6488):354–357, 1994.

[12] BO Dabbousi, MG Bawendi, O Onitsuka, and MF Rubner. Electroluminescence from cdse quantum-dot/polymer composites. *Appl. Phys. Lett.*, 66(11):1316–1318, 1995.

[13] PJ Dean. Comparison of mocvd-grown with conventional ii-vi materials parameters for el thin films). *Phys. Status Solidi A*, 81(2):625–646, 1984.

[14] Yong Joo Doh, Kristin N. Maher, Lian Ouyang, Chun L. Yu, Hongkun Park, and Jiwoong Park. Electrically driven light emission from individual cdse nanowires. *Nano Lett.*, 8(12):4552–4556, 2008.

[15] August Dorn, Hao Huang, and Moungi G Bawendi. Electroluminescence from nanocrystals in an electromigrated gap composed of two different metals. *Nano Lett.*, 8(5):1347–1351, 2008.

[16] Xiangfeng Duan, Yu Huang, Yi Cui, Jianfang Wang, and Charles M Lieber. Indium phosphide nanowires as building blocks for nanoscale electronic and optoelectronic devices. *Nature*, 409(6816):66–69, 2001.

[17] A. A. Grinberg and Serge Luryi. Space-charge-limited current and capacitance in double-junction diodes. *J. Appl. Phys.*, 61(3):1181–1189, feb 1987.

[18] Mark S Gudiksen, Kristin N Maher, Lian Ouyang, and Hongkun Park. Electroluminescence from a single-nanocrystal transistor. *Nano Lett.*, 5(11):2257–61, 2005.

[19] Christopher Hahn, Zhaoyu Zhang, Anthony Fu, Cheng Hao Wu, Yun Jeong Hwang, Daniel J. Gargas, and Peidong Yang. Epitaxial growth of ingan nanowire arrays for light emitting diodes. *ACS Nano*, 5(5):3970–3976, MAY 2011.

[20] W. Chuck Hsu, Jun-Yi Chyan, Yen-Sheng Lu, and J. Andrew Yeh. Electroluminescence of out-of-plane silicon nanowire/silver oxide/silver nanodendrite heterostructures. *Opt. Mater. Express*, 1(7):1210–1215, NOV 1 2011.

[21] Y Huang, XF Duan, and CM Lieber. Nanowires for integrated multicolor nanophotonics. *Small*, 1(1):142–147, JAN 2005.

[22] Bong Hoon Kim, M Serdar Onses, Jong Bin Lim, Sooji Nam, Nuri Oh, Hojun Kim, Ki Jun Yu, Jung Woo Lee, Jae-Hwan Kim, Seung-Kyun Kang, et al. High-resolution patterns of quantum dots formed by electrohydrodynamic jet printing for light-emitting diodes. *Nano Lett.*, 15(2):969–973, 2015.

[23] Kwangeun Kim, Jeongmin Kang, Myeongwon Lee, Changjoon Yoon, Kyoungah Cho, and Sangsig Kim. Ultraviolet electroluminescence emission from n-type zno/p-type si crossed nanowire light-emitting diodes. *Jpn. J. Appl. Phys.*, 49:06GG05, 2010.

[24] Sheng-Chin Kung, Wytze E. van der Veer, Fan Yang, Keith C. Donavan, and Reginald M. Penner. 20 microsecond photocurrent response from lithographically patterned nanocrystalline cadmium selenide nanowires. *Nano Lett.*, 10(4):1481–1485, 2010.

[25] Sheng-Chin Kung, Wendong Xing, Wytze E van der Veer, Fan Yang, Keith C Donavan, Ming Cheng, John C Hemminger, and Reginald M Penner. Tunable photoconduction sensitivity and bandwidth for lithographically patterned nanocrystalline cadmium selenide nanowires. *ACS Nano*, 5(9):7627–7639, 2011.

[26] Murray A. Lampert. Simplified theory of space-charge-limited currents in an insulator with traps. *Phys. Rev.*, 103(6):1648–1656, sep 1956.

[27] Guangru Li, Florencia Wisnivesky Rocca Rivarola, Nathaniel JLK Davis, Sai Bai, Tom C Jellicoe, Francisco de la Peña, Shaocong Hou, Caterina Ducati, Feng Gao, Richard H Friend, et al. Highly efficient perovskite nanocrystal light-emitting diodes enabled by a universal crosslinking method. *Adv. Mater.*, 2016.

[28] Gong-Ru Lin, Chun-Jung Lin, Chi-Kuan Lin, Li-Jen Chou, Yu-Lun Chueh, and and others. Oxygen defect and si nanocrystal dependent white-light and near-infrared electroluminescence of si-implanted and plasma-enhanced chemical-vapor deposition-grown si-rich sio2. *J. Appl. Phys.*, 97(9):094306, 2005.

[29] C. Y. Liu, H. Y. Xu, J. G. Ma, X. H. Li, X. T. Zhang, Y. C. Liu, and R. Mu. Electrically pumped near-ultraviolet lasing from zno/mgo core/shell nanowires. *Appl. Phys. Lett.*, 99(6):063115 (3 pp), AUG 8 2011.

[30] Benjamin S Mashford, Matthew Stevenson, Zoran Popovic, Charles Hamilton, Zhaoqun Zhou, Craig Breen, Jonathan Steckel, Vladimir Bulovic, Moungi Bawendi, Seth Coe-Sullivan, et al. High-efficiency quantum-dot light-emitting devices with enhanced charge injection. *Nat. Photonics*, 7(5):407–412, 2013.

[31] Michael C McAlpine, Robin S Friedman, Song Jin, Keng-hui Lin, Wayne U Wang, and Charles M Lieber. High-performance nanowire electronics and photonics on glass and plastic substrates. *Nano Lett.*, 3(11):1531–1535, 2003.

[32] EJ Menke, MA Thompson, C Xiang, LC Yang, and RM Penner. Lithographically patterned nanowire electrodeposition. *Nat. Mater.*, 5(11):914–919, 2006.

[33] N. F. (Nevill Francis) Sir Mott and Ronald W. (Ronald Wilfrid) Gurney. *Electronic Processes in Ionic Crystals*. Oxford : Clarendon Press, 2nd ed edition, 1948.

[34] Gerd Mueller. *Electroluminescence II*. San Diego, CA : Academic Press, 2000.

[35] PN Murgatroyd. Theory of space-charge-limited current enhanced by frenkel effect. *J. Phys. D Appl. Phys.*, 3(2):151, 1970.

[36] Atsushi Nitta, Kenji Tanaka, Yoshiharu Maekawa, Minoru Kusabiraki, and Masao Aozasa. Effects of gas impurities in the sputtering environment on the stoichiometry and crystallinity of zns: Mn electroluminescent-device active layers. *Thin Solid Films*, 384(2):261–268, 2001.

[37] Ryo Nouchi. Extraction of the schottky parameters in metal-semiconductor-metal diodes from a single current-voltage measurement. *J. Appl. Phys.*, 116(18):184505, 2014.

[38] AO Oduor and RD Gould. A comparison of the dc conduction properties in evaporated cadmium selenide thin films using gold and aluminium electrodes. *Thin Solid Films*, 317(1):409–412, 1998.

[39] Jozef Osvald. Back-to-back connected asymmetric schottky diodes with series resistance as a single diode. *Phys. Status Solidi A*, 212(12):2754–2758, 2015.

[40] Bhola N Pal, Yagnaseni Ghosh, Sergio Brovelli, Rawiwan Laocharoensuk, Victor I Klimov, Jennifer A Hollingsworth, and Han Htoon. 'giant' cdse/cds core/shell nanocrystal quantum dots as efficient electroluminescent materials: Strong influence of shell thickness on light-emitting diode performance. *Nano Lett.*, 12(1):331–336, 2011.

[41] Reginald M. Penner. Electrodeposited nanophotonics. *J. Phys. Chem. C*, 118(31):17179–17192, 2014.

[42] Om Prakash, K N Muralidhara, and K Ravindra. Rectifying contacts on cdse films. *IETE Tech. Rev.*, 7(4):260–263, 1990.

[43] M. W. J. Prins, K.-O. Grosse-Holz, J. F. M. Cillessen, and L. F. Feiner. Grain-boundary-limited transport in semiconducting SnO2 thin films: Model and experiments. *J. Appl. Phys.*, 83(2):888–893, jan 1998.

[44] Fang Qian, Silvija Gradecak, Yat Li, Cheng-Yen Wen, and Charles M Lieber. Core/multishell nanowire heterostructures as multicolor, high-efficiency light-emitting diodes. *Nano Lett.*, 5(11):2287–2291, 2005.

[45] A. Rose. Space-charge-limited currents in solids. *Phys. Rev.*, 97(6):1538–1544, mar 1955.

[46] Michael A Schreuder, Kai Xiao, Ilia N Ivanov, Sharon M Weiss, and Sandra J Rosenthal. White light-emitting diodes based on ultrasmall cdse nanocrystal electroluminescence. *Nano Lett.*, 10(2):573–576, 2010.

[47] KN Sharma and K Barua. Electrical properties of evaporated cdse films. *J. Phys. D Appl. Phys.*, 12(10):1729, 1979.

[48] Yasuhiro Shirasaki, Geoffrey J Supran, Moungi G Bawendi, and Vladimir Bulović. Emergence of colloidal quantum-dot light-emitting technologies. *Nat. Photonics*, 7(1):13–23, 2013.

[49] J.G. Simmons. Poole-frenkel effect and schottky effect in metal-insulator-metal systems. *Phys. Rev.*, 155(3):657, 1967.

[50] JG Simmons. Conduction in thin dielectric films. *J. Phys. D Appl. Phys.*, 4(5):613, 1971.

[51] Subhojyoti Sinha, Sanat Kumar Chatterjee, Jiten Ghosh, and Ajit Kumar Meikap. Electrical transport properties of polyvinyl alcohol–selenium nanocomposite films at and above room temperature. *J. Mater. Sci.*, 50(4):1632–1645, 2015.

[52] Subhojyoti Sinha, Sanat Kumar Chatterjee, Jiten Ghosh, and Ajit Kumar Meikap. Semiconducting selenium nanoparticles: Structural, electrical characterization, and formation of a back-to-back schottky diode device. *J. Appl. Phys.*, 113(12), 2013.

[53] Nicolas Sommer, Jrgen Hpkes, and Uwe Rau. Field emission at grain boundaries: Modeling the conductivity in highly doped polycrystalline semiconductors. *Phys. Rev. Appl.*, 5(2), feb 2016.

[54] Geoffrey J Supran, Yasuhiro Shirasaki, Katherine W Song, Jean-Michel Caruge, Peter T Kazlas, Seth Coe-Sullivan, Trisha L Andrew, Moungi G Bawendi, and Vladimir Bulović. Qleds for displays and solid-state lighting. *MRS bulletin*, 38(09):703–711, 2013.

[55] S. M. Sze and Kwok Kwok Ng. *Physics of Semiconductor Devices*. Wiley-Interscience, Hoboken, N.J., 3rd ed edition, 2007.

[56] SM Sze, DJ Coleman, and A Loya. Current transport in metal-semiconductor-metal (msm) structures. *Solid State Electron.*, 14(12):1209–1218, 1971.

[57] Katsuhiro Tomioka, Junichi Motohisa, Shinjiroh Hara, Kenji Hiruma, and Takashi Fukui. Gaas/algaas core multishell nanowire-based light-emitting diodes on si. *Nano Lett.*, 10(5):1639–1644, MAY 2010.

[58] SK Tripathi. Temperature-dependent barrier height in cdse schottky diode. *J. Mater. Sci.*, 45(20):5468–5471, 2010.

[59] Chengxiang Xiang, Yongan Yang, and Reginald M Penner. Cheating the diffraction limit: Electrodeposited nanowires patterned by photolithography. *Chem. Commun.*, (8):859–873, 2009.

[60] Wendong Xing, Wenbo Yan, Talin Ayvazian, Yong Wang, Eric O Potma, and Reginald M Penner. Electrodeposited light-emitting nanojunctions. *Chem. Mater.*, 25(4):623–631, 2013.

[61] Ruoxue Yan, Daniel Gargas, and Peidong Yang. Nanowire photonics. *Nat. Photonics*, 3(10):569–576, 2009.

[62] Peidong Yang, Ruoxue Yan, and Melissa Fardy. Semiconductor nanowire: What's next? *Nano Lett.*, 10(5):1529–1536, 2010.

[63] Xuyong Yang, Evren Mutlugun, Cuong Dang, Kapil Dev, Yuan Gao, Swee Tiam Tan, Xiao Wei Sun, and Hilmi Volkan Demir. Highly flexible, electrically driven, top-emitting, quantum dot light-emitting stickers. *ACS Nano*, 8(8):8224–8231, 2014.

[64] Yu Ye, Lin Gan, Lun Dai, Hu Meng, Feng Wei, Yu Dai, Zujin Shi, Bin Yu, Xuefeng Guo, and Guogang Qin. Multicolor graphene nanoribbon/semiconductor nanowire heterojunction light-emitting diodes. *J. Mater. Chem.*, 21(32):11760–11763, 2011.

[65] Wenjin Zhang, Qing Lou, Wenyu Ji, Jialong Zhao, and Xinhua Zhong. Color-tunable highly bright photoluminescence of cadmium-free cu-doped zn–in–s nanocrystals and electroluminescence. *Chem. Mater.*, 26(2):1204–1212, 2013.

[66] Jialong Zhao, Julie A Bardecker, Andrea M Munro, Michelle S Liu, Yuhua Niu, I-Kang Ding, Jingdong Luo, Baoquan Chen, Alex K-Y Jen, and David S Ginger. Efficient cdse/cds quantum dot light-emitting diodes using a thermally polymerized hole transport layer. *Nano Lett.*, 6(3):463–467, 2006.

[67] ZH Zhong, F Qian, DL Wang, and CM Lieber. Synthesis of p-type gallium nitride nanowires for electronic and photonic nanodevices. *Nano Lett.*, 3(3):343–346, MAR 2003.

[68] Mariano A. Zimmler, Jiming Bao, Ilan Shalish, Wei Yi, Venkatesh Narayanamurti, and Federico Capasso. A two-colour heterojunction unipolar nanowire light-emitting diode by tunnel injection. *Nanotechnology*, 18(39):395201 (8 pp), OCT 3 2007.

[69] Mariano A. Zimmler, Tobias Voss, Carsten Ronning, and Federico Capasso. Exciton-related electroluminescence from zno nanowire light-emitting diodes. *Appl. Phys. Lett.*, 94(24):241120 (3 pp), JUN 15 2009.